PCCP

Cite this: *Phys. Chem. Chem. Phys.*, 2012, **14**, 13058–13066

www.rsc.org/pccp

PAPER

Electronic excitations of C_{60} aggregates

A. L. Montero-Alejo,*[ab] E. Menéndez-Proupin,*[bc] M. E. Fuentes,[d] A. Delgado,[ef] F.-P. Montforts,[g] L. A. Montero-Cabrera[a] and J. M. García de la Vega[b]

Received 13th June 2012, Accepted 19th July 2012
DOI: 10.1039/c2cp41979c

Excitation properties of the isolated C_{60} and $(C_{60})_N$ model clusters (N = 2, 3, 4, 6 and 13) are studied using an *a priori* parameterized and self-consistent Hamiltonian, the Complete Neglect of Differential Overlap considering the *l* azimuthal quantum number method. This method properly describes electron excitations of the isolated C_{60} after the configuration interaction of singles (CIS) procedure, when those are compared with experimental data in *n*-hexane solution and in a molecular beam. Geometry models of $(C_{60})_N$ clusters to model the effect of aggregation were obtained from the fullerene fcc crystal. Some peaks in the low energy edge of the absorption spectrum appear corresponding to clustering effects, as well as small increases of bandwidths in the strong bands at the UV region. An analysis of the theoretical absorption spectrum for dimer models has been carried out, taking into account the influence of the distance between fullerene centers. The density of states of CIS for fullerene clusters in the range from 2.0 to 6.5 eV shows the possibility of electron transitions as functions of the size of the clusters.

1. Introduction

The Buckminsterfullerene C_{60} and similar carbon ball-shaped molecules appear to be the building blocks of molecular complexes and extended solids with many potential applications, being subjects of thousands of articles since their discovery. Such applications[1–8] include photovoltaic devices, hydrogen storage and nanomedicine. The electronic transitions and states of C_{60} fullerene have been intensively studied by a combination of experimental and theoretical techniques.[9–23] An intense community effort has led to an understanding of the low energy part of the excitation spectrum, which has been probed mainly by fluorescence spectroscopy combined with other techniques (see ref. 9 and references therein). Higher energy excitations have been probed by visible and UV light absorption. For this range of excitations, the simulation effort has been less intense and agreement with experiment is less satisfactory, as discussed below.

[a] *Laboratorio de Química Computacional y Teórica, Facultad de Química, Universidad de la Habana, 10400 Havana, Cuba. E-mail: analilian.montero@fq.uh.cu, ana.montero@uam.es*
[b] *Departamento de Química Física Aplicada, Facultad de Ciencias, Universidad Autónoma de Madrid, 28049 Madrid, Spain*
[c] *Grupo de Nanomateriales, Departamento de Física, Facultad de Ciencias, Universidad de Chile, Las Palmeras 3425, 780-0024 Ñuñoa, Santiago, Chile*
[d] *Laboratorio de Química Computacional, Universidad Autónoma de Chihuahua, 31000 Chihuahua, México*
[e] *CNR-NANO S3, Institute for Nanoscience, Via Campi 213/A - 41125, Modena, Italy*
[f] *Centro de Aplicaciones Tecnológicas y Desarrollo Nuclear (CEADEN), Calle 30 # 502, 11300 La Habana, Cuba*
[g] *Institut für Organische Chemie, FB 2, Universität Bremen, Postfach 33 04 40, 28359, Bremen, Germany*

Optical absorption spectra have been reported for C_{60} in gas phase at high temperatures,[12,24] resulting in broad spectral features and the interpretation is complicated because of the presence of abundant vibronic states. Low and room temperature optical spectra have been reported for thin films,[17,18] and in solution of *n*-hexane,[10] water,[25] liquid helium,[15] and noble gas solid matrices.[13] The study of fullerene in *n*-hexane solution by Leach *et al.*[10] provides the most detailed characterization of the UV optical spectrum. Three strong absorption bands dominate this spectrum with peaks at 3.78, 4.84 and 5.88 eV. The remarkable similarity of these band patterns in different media suggests that they represent the "fingerprint" of the isolated C_{60} spectrum. However, the optical spectra of C_{60} in aqueous phase and in thin solid films are distinguished because all of the bands appear wider with respect to that obtained in gas and hydrocarbon media. Moreover, a broad and weak absorption band in the range 2.3–3.0 eV appears in the spectra of C_{60} water solutions and thin films. Interpretations of these spectral differences have been proposed as a powerful tool to investigate the properties of the stable C_{60} colloidal suspensions because of their environmental fate.[26,27]

Up to now, experimental results have been mostly interpreted with the help of calculations for isolated molecules. It is well known that the excited electronic states that mediate the optical response present a strong correlation, and must be described by methods beyond ground state mean field approximations like Hartree–Fock and Density functional (DFT) theory.[28,29] Nowadays, time-dependent density functional theory (TDDFT)[30] has become a standard tool for investigating excitations in large molecules, and it has been shown to describe reasonably well optical

absorptions in C_{60}.[28,31,32] The correlated excited states have also been studied with many-particle wave-function methods, especially with semi empirical variants with configuration interaction (CI) procedures. Orlandi and Negri[9] have reviewed the assignment of the UV-vis absorption bands guided by the semi empirical method of complete neglect of differential overlap for spectroscopy (CNDO/S).[33] CNDO/S was also useful to understand the infrared and the red edge spectrum, as well as the fluorescence, which are dominated by vibronic transitions to dipole-forbidden states.[9,19,34] A common drawback of published calculations based on wavefunction methods is that the calculated electronic excitation energies appear overestimated. This is commonly attributed to the approximation of using single excited configurations (SECs) for the CI treatment,[9] as well as the use of limited basis sets for the reference ground states. However, double excitations have been included in CNDO/S calculations by Hara *et al.*[35] and they have been shown to increase the gap between the ground and the excited states.

TDDFT results, considering either adiabatic generalized gradient approximation (GGA)[31,36] or local density approximation (LDA)[37] functionals, show a semiquantitative description of the same experimental data in *n*-hexane solution.[10] In an early GGA report,[31] the modeled spectrum was corrected by adding a 0.35 eV blueshift in order to match the bands with the experimental data. Later TDDFT calculations[32,36] with different basis sets and different computational approaches provided results that were consistent, although they underestimated transition energies. The same trend has also been reported by considering the self-consistent Extended Hückel (SC-EH) theory as an approximation of the Kohn–Sham density functional in the evaluations of the TD-DFT response kernel.[38] A promising route to improve the excitation energies, yet to be tested for the C_{60} spectrum, is the use of range-separated hybrid functionals.[39,40]

The *ab initio* single excited configuration interaction (CIS) treatment of C_{60} molecule provides a different picture of the electron transition spectrum.[41] The two lowest allowed electronic excitations have been computed at relatively high values (5.8 and 6.3 eV), which are in the energy range of only one of the experimental bands. The density of CIS states (DOS-CIS) obtained from this calculation was used to suggest the possible vibronic origin of the bands between 3.0 and 5.0 eV. However, the shape of the resulting bands differs from experimental data, and electron transitions below 3.2 eV are not predicted, which is contradictory to the rest of the theoretical studies.

The experimental spectrum shows other broad bands that are unassigned. The nature of non-assigned transitions should be examined through the expected activation of forbidden electronic states by vibronic effects, by possible multiple-electron excitations, and by interactions with the molecular environment or nearby C_{60}s (aggregation effects). A simulation of these effects involves a great computational effort that is unreachable by *ab initio* methods nowadays, opening the field for suitable semiempirical methods.[7] On the other hand, the actual research studies for fullerene applications demand the modeling of supramolecular complexes with a prohibitive number of atoms, such as electron donor–acceptor ensembles[6,8,42–44] and nanoclusters of carbon[2] which are candidates for developing efficient photoelectrochemical and photovoltaic cells. In this context, the CNDO/S method has already been used to study the nature of the electronic excitations of a van der Waals dimer of C_{60}.[45]

The above mentioned facts reinforce the necessity of further theoretical modeling of C_{60} and its environment. On one hand, it is necessary to improve the quantitative interpretation of the experimental results. On the other hand, the theoretical method must be scalable to systems of thousands of atoms, and both aspects should be developed in parallel progression. In the present work we present a study of the optical absorption spectrum of isolated C_{60} molecules and $(C_{60})_N$ model clusters (N = 2, 3, 4, 6 and 13) by the CNDOL method. CNDOL is an approximate quantum mechanical Hamiltonian[46] that considers all valence interacting electrons. It represents a good starting point for building a molecular wave function of relatively big systems.[47,48] Recently, the optical properties of single walled carbon nanotubes with more than 8 nm length were predicted,[49] opening the possibility to study non-regular objects at a nanoscopic scale using a reliable quantum mechanical tool. Here, we analyze the fullerene absorption spectrum between 2.5 and 6 eV, with emphasis on the three strong absorption bands and on the fine structure of the spectrum edge. We find that the absorption edge is sensitive to the interaction between neighboring C_{60} units and provides signatures of aggregation effects.

2. Model and methods

CNDOL mimics the Hartree–Fock–Roothaan (HFR) equations with minimal basis sets of Slater orbitals, replacing the mono-electronic and bielectronic integrals with appropriate estimation formulae. The single-particle equations are solved self-consistently, and the excited states are constructed in the CIS manner. CNDOL shares many aspects with CNDO/S. It differs from CNDO/S in two essential aspects. The CNDOL valence atomic basis is augmented (improved the quality) while considering its azimuthal quantum number (l), and all of the parameters used are chosen *a priori* avoiding any adjustment with specific data sets.

The electronic excited states are resolved in two steps. First, the single particle molecular orbitals are calculated by the self-consistent solution of the CNDOL/21 Hamiltonian.[47] In the second step, the excited states are found using the CIS method (see below). The CNDOL/21 Hamiltonian is defined in terms of a minimal basis set of atomic orbitals ϕ_μ, ϕ_ν. For each carbon atom, there are four Slater orbitals of symmetry s, p_x, p_y, and p_z, which correspond to the valence shell. The matrix elements of the CNDOL/21 Hamiltonian can be cast as

$$F_{\mu\mu} = -\frac{1}{2}(I_l + A_l) + \frac{1}{2}\gamma_{ll}^{AA} - \sum_{k=s,p} Z_k^A \gamma_{lk}^{AA} - \sum_{B\neq A}\sum_{k=s,p} Z_k^B \gamma_{lk}^{AB} - \frac{1}{2} P_{\mu\mu}\gamma_{ll}^{AA} + \sum_{B\neq A}\sum_{k=s,p} P_k^B \gamma_{lk}^{AB} \quad (1)$$

$$F_{\mu\nu} = -\frac{1}{2}(I_l + I_{l'})S_{\mu\nu} - \frac{1}{2} P_{\mu\nu}\gamma_{ll'}^{AB} \quad (2)$$

In eqn (1) and (2), l = s or p, denotes the symmetry of the orbital ϕ_μ, and l′ the symmetry of ϕ_ν. The letter A refers to the atom where the orbital ϕ_μ is centered, while B refers to other atoms.

I_l and A_l are the experimental ionization potential and affinity of the atomic shell l. The symbols $\gamma_{ll'}^{AB}$ denote the non-null Coulomb bi-electronic integrals, that are expressed in terms of I_l and A_l, and the interatomic distance, as explained below. Z_k^A is the k-subshell valence charge in the atomic reference state, $P_{\mu\nu}$ is the density matrix, and P_k^A is the sum of $P_{\mu\mu}$ in the k-subshell of atom A. The first three terms in eqn (1) represent the electron kinetic energy and the interaction with the core of the same atom (Pople and Segal),[50] the following summation stands for the interaction with other cores (of atoms B), and the terms containing the density matrix represent the electron–electron interaction. The term $S_{\mu\nu}$ in eqn (2) denotes the overlap matrix between the basis functions.

The parameterization of the bi-electronic integrals varies across the family of CNDO methods. In this work, the two-center repulsion integral expression corresponds to a modification of the Mataga–Nishimoto[51,52] formula

$$\gamma_{lk}^{AB} = \left[\frac{a_{AB}^{lk} R_{AB}}{(a_{AB}^{lk} + R_{AB})^2}\right], \text{where } a_{AB}^{lk} = \frac{2}{(\gamma_{ll}^{AA} + \gamma_{kk}^{BB})}. \quad (3)$$

The bi-centric terms γ_{lk}^{AB} decrease as $1/R_{AB}$ when R_{AB} tends to infinity. The electron pair repulsion in a center A (γ_{ll}^{AA}) is evaluated by Pariser's relation[53] as is traditional for this method.

The CIS algorithm is divided into three main steps: (i) generation and selection of which SECs will be considered, (ii) calculation of the CIS matrix, and (iii) diagonalization. By a SEC $|i \rightarrow k\rangle$, we understand a many-electron state obtained from the ground state Slater determinant, replacing one occupied molecular orbital i by an unoccupied k one. This can be regarded as a one-electron transition from a low to a high energy orbital. The energy of the SEC is the diagonal matrix element of the many-electron Hamiltonian. The general matrix element of the CIS Hamiltonian for singlet states is given as[54]

$$\langle i \rightarrow k|\mathrm{H}|j \rightarrow l\rangle = \delta_{ij}\delta_{kl}(\varepsilon_k - \varepsilon_i) - \langle jk|il\rangle + 2\langle jk|li\rangle, \quad (4)$$

where $(\varepsilon_k - \varepsilon_i)$ is the difference of the two implied molecular orbital energies (single-particle term), and $-\langle jk|il\rangle$ and $2\langle jk|li\rangle$ are the Coulomb and exchange interactions respectively (two-particle term).

The selection of our active space, *i.e.*, the set of self-consistent orbitals that span the SECs, is crucial to calculate the spectra. If N_1 occupied and N_2 unoccupied orbitals are chosen, the number of SECs is $N_1 \times N_2$. CNDO/S and other CIS quantum chemistry methods use active spaces that tend to contain equal number of occupied and empty orbitals. Different CNDO/S studies of C_{60} illustrate the variations in the calculated spectra with the number of SECs. The largest number of SECs considered in those CNDO/S calculations[34] was $35 \times 37 = 1295$, out of $120 \times 120 = 14\,400$ possible SECs for one molecule of C_{60} with minimal atomic basis.

In a full CIS calculation of C_{60} we employ a different scheme for defining the SECs basis set. All the possible SECs are generated and calculated their energies, *i.e.*, the diagonal elements of the CIS matrix. Then, these SECs are sorted in ascending order of energy, and the CIS basis is selected with all the SECs with energy smaller than or equal to a predefined cutoff limit. Therefore, this energy cutoff is the only parameter that controls the number of SECs. This procedure clearly offers a balanced basis in the case of pronounced disparities in the density of states of occupied and unoccupied levels. To avoid a too incomplete CIS basis, we also include SECs with larger energy than the cutoff, although showing monoelectronic wavefunction eigenvalue $(\varepsilon_k - \varepsilon_i)$ differences smaller than or equal to the SECs below the cutoff. In other words, the energies of all the SECs included in the CIS basis are below an explicitly defined cutoff, or show a single particle term below the other, implicitly defined, cutoff. In the particular case of fullerene, this correction allows a complete inclusion of certain combinations of occupied and excited orbitals that are degenerate as single particle states, although split due to electron interaction terms when combined to form SECs. For C_{60}, a cutoff of 13.2 eV provides a reasonable tradeoff between the full CIS spectrum and a low computational cost (see Fig. A1 in Appendix A). The same cutoff has been used for the $(C_{60})_N$ clusters, except for the largest model ($(C_{60})_{13}$) where a 7.2 eV cutoff was used to appropriately describe only the low energy transitions.

It must be considered that all possible SECs do not necessarily optimize the calculated results since we are not including the contribution of multiply excited determinants to the system wavefunction, and therefore it would remain far from full CI. Another important reason is that the limited (minimal) atomic basis set implicit in approximate HF Hamiltonians used to build the molecular one electron wave functions should be far from complete. In particular, extended states of the continuum spectrum cannot be accounted.

The CNDOL description of the studied system will be presented in the order of degrees of aggregation. First, we show results of the low-energy excited states (below 6.5 eV) of isolated C_{60} molecules as predicted by our method. The results are compared with the experimental absorption spectrum and with other theoretical predictions. Second, we show results on the absorption spectra of dimers $(C_{60})_2$ as a function the center–center distance. Finally, we present model absorption spectra of the heavier cluster models such as $(C_{60})_3$, $(C_{60})_4$, $(C_{60})_6$ and $(C_{60})_{13}$. For the sake of comparison, reported intensities of all $(C_{60})_N$ calculated absorption spectra have been normalized to a single C_{60} unit, *i.e.*, divided by N.

The structural model of C_{60} was taken from the face centered cubic crystal structure[55] and it was relaxed using DFT calculations. The plane-wave pseudopotential Quantum ESPRESSO package[56] was used. The exchange and correlation parts of the electronic energy were calculated with the GGA functional of Perdew, Burke and Ernzerhof (PBE).[57] The pseudopotential C.pbe-rrkjus.UPF from the Quantum-ESPRESSO distribution was used. Kinetic energy cutoffs of 30 Ry and 320 Ry were used for the expansion of the wave functions and the charge density, respectively. The wave function was obtained at the gamma point. To avoid convergence problems, the method of cold smearing[58] was used, with a broadening parameter of 0.01 Ry. The structure was relaxed using the BFGS quasi-Newton algorithm. Auxiliary relaxations were made for a C_{60} molecule in a 20 Å wide cubic supercell. The effects of using a correction for dispersion forces and a different pseudopotential were tested and shown to be small.

The resulting two different C–C bond lengths, $R_{C-C} = 1.45$ Å (in pentagons) and $R_{C=C} = 1.39$ Å (in hexagons), fit the

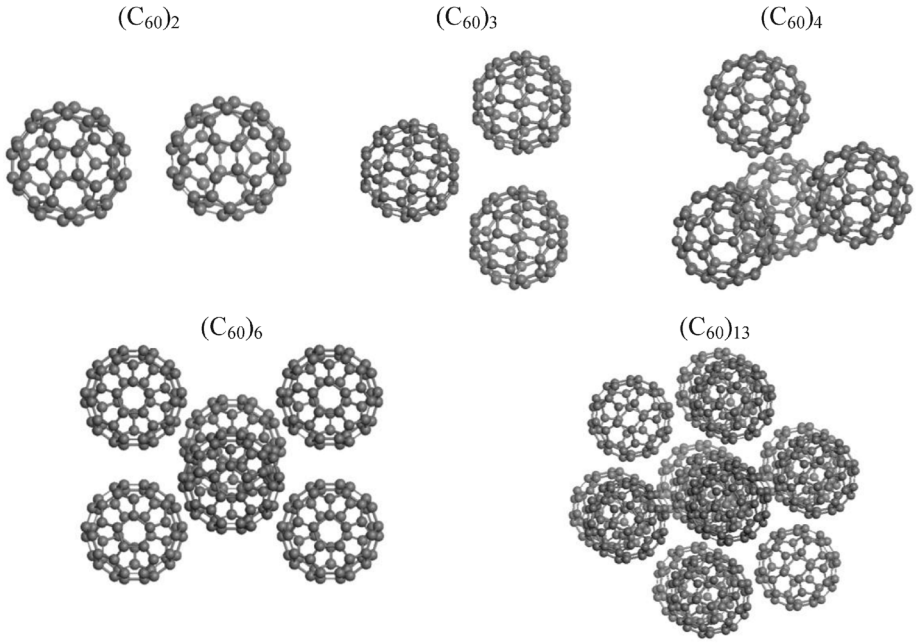

Fig. 1 Structural arrangements of the $(C_{60})_N$ cluster models. The distance between neighboring C_{60} molecules (fullerene center–center) in the crystal is 10.02 Å.

reported experimental geometry of this molecule of 1.46 and 1.40 Å for gas phase[9,59] and of 1.46 and 1.38 Å for the room temperature crystal structure.[60] The center–center distance (R) between neighboring C_{60} molecules in the crystal is 10.02 Å, which agree with a previous report.[61] The $(C_{60})_N$ cluster models were built by replication of the C_{60} molecule at fcc lattice vectors. In the case of the trimer $(C_{60})_3$, tetramer $(C_{60})_4$ and tridecamer $(C_{60})_{13}$, fullerenes were extracted in triangular, tetrahedral and icosahedral shapes respectively. A non-regular octahedral form was achieved for the $(C_{60})_6$ model. In addition, other dimer models $(C_{60})_2$ were obtained by increasing R from the original in the crystal dimer (10.02 Å) up to 13.02 Å. Fig. 1 shows the structural arrangements of these molecular clusters.

3. Results and discussion

3.1. C_{60} results

Table 1 displays detailed information on the calculated optical transitions in the UV-vis spectrum, as grouped from analysis of experimental data. The oscillator strengths of the TDDFT calculation[31] have been multiplied by three, in order to account for the triple degeneration of T_{1u} levels and to compare with the experimental values. We verified that this is the case after doing our own TDDFT calculation. The reported TDDFT calculations give too low oscillator strengths (theoretical intensities derived from transition dipoles) compared with the experiments, and CNDO/S gives too high values. In the case of CNDO/S, it is believed that these high oscillator strengths can be reduced with the inclusion of double excitations in the CI expansion.[62]

Fig. 2 shows the C_{60} absorption spectrum calculated with different methods, and two representative experimental spectra. The theoretical absorption spectrum has been simulated by the convolution of Lorentzian functions multiplied by the oscillator

Table 1 Transition energies E and strengths f obtained by different levels of theory

CNDO/S[a] E; f	CNDO/S[b] E; f	TDDFT[c] E; f	CNDOL[d] (cutoff) E; f	CNDOL[d] (Full CIS) E; f
3.4; 0.08	3.4; 0.12	2.82; 0.006	3.00; 0.003	2.98; 0.003
4.06; 0.41	4.02; 0.54	3.51; 0.417	**3.82; 0.429**	**3.74; 0.447**
4.38; 2.37	**4.28; 2.70**	**4.48; 1.107**	4.54; 0.081	4.52; 0.141
4.70; 0.3	4.64; 0.54	5.02; 0.000		
5.07; ---	**5.03; 2.94**	5.10; 0.009	**4.81; 1.02**	**4.71; 0.75**
5.24; 7.88	**5.20; 5.79**	**5.47; 2.295**	4.93; 0.021	4.92; 0.012
			5.13; 0.060	5.12; 0.033
5.54; 1.18	5.51; 0.81	5.72; 0.024	5.49; 0.015	5.47; 0.033
			5.68; 0.030	5.66; 0.045
5.78; 10.74	**5.62; 3.21** 6.31; 0.42	**5.98; 2.438**	**6.27; 2.10**	**6.09; 1.71**

[a] Ref. 62. [b] Ref. 9. [c] Ref. 31. The f are multiplied by 3 to account for degeneration (see the text). [d] This work. The cutoff is 13.2 eV.

strength of each electronic excitation. The peaks of the spectra are labelled a, c, e, and g, and the shoulders f and h, following the notation of Bauernschmitt *et al.*[31] The b and d broad bands also appear which have neither been resolved nor assigned to any particular electronic transition. We found no clear experimental reference to establish what theoretical method is more accurate in terms of excitation energies and peak intensities. Theoretical calculations should be ideally compared with low temperature spectra of C_{60} in gas phase. However, we have only found gas phase measurements made at high temperature clearly showing the effects of thermal dilation and strong broadening due to thermal motion. Moreover, the uncertainty in the determination of the gas density affects the absolute cross section values.[24] On the other hand, low temperature measurements for C_{60} in liquid and solid matrices are influenced by the environment. Sassara *et al.*[13] (and references cited therein) have correlated the main spectral

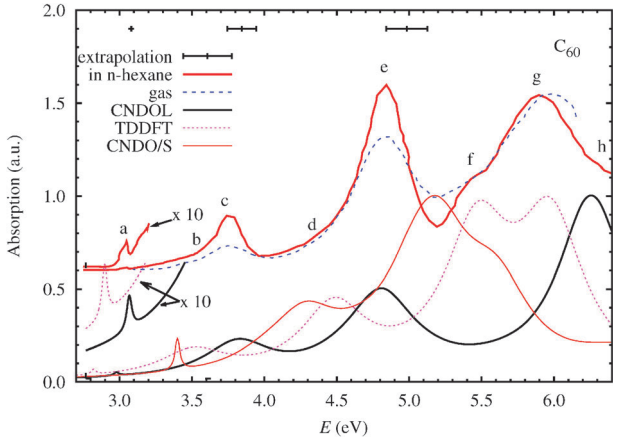

Fig. 2 Experimental and theoretical absorption spectra of C_{60}. The experimental values are reported in *n*-hexane solution at 300 K[10] and from a molecular beam at an estimated temperature of 973 K.[12] Calculations are made with CNDOL (this work), TDDFT,[31] and CNDO/S[34] methods. Horizontal error bars represent the extrapolated peak energies and bandwidths as estimated for a cold gas phase spectrum.[13]

features (peak wavelengths and linewidths) with certain physical properties of the solvents, *e.g.* the Lorentz–Lorenz polarizability, and have extrapolated to the dielectric parameters of vacuum thus estimating the main spectral features in a cold gas phase. The extrapolated peak energies and linewidths are indicated by horizontal error bars in Fig. 2 at the top of the experimental spectra. It turns out that the peak energies in hot gas phase[12] are very close to the values in *n*-hexane at room temperature,[10] and in both cases the peaks are red-shifted with respect to the estimated cold gas phase absorption.[13] Nevertheless, the redshifts are smaller than 0.2 eV and this magnitude is smaller than the expected accuracy of any theoretical method. Hence, we will use the reliable *n*-hexane experiment[10] as reference.

Another issue is the fact that bandwidths are non-uniform, and although one can simulate the spectra using fitted values, it makes difficult the comparison between different methods. For example, Bauernschmitt *et al.*[31] corrected their spectra (TDDFT in Fig. 2) with a blue-shift of 0.35 eV to achieve better agreement with experimental energies. In particular, this improves the agreement for peaks a and c, but changes the assignment of peak g between the double peak structure at 5.5 and 5.9 eV. If the TDDFT spectrum is not blue-shifted (taken "as is"), the f and g structures can be assigned to transitions to the 6^1T_{1u} and 8^1T_{1u} states, respectively. However, if the blue-shifted spectrum is taken, then 6^1T_{1u} must be assigned to peak g, and 8^1T_{1u} to peak h.[31] Hence, one should assign different linewidths to these transitions depending on whether a shift is applied to the energies. Moreover, if one applies shifts for every theoretical method and fits bandwidths biasing the comparison is unavoidable. Therefore, we prefer to compare the spectra with the energies without any *a posteriori* correction, and to choose the same bandwidth 0.27 eV to simulate all and each calculated transition. This band width is the same as that used by Rocca *et al.*,[36] who reported a very similar TDDFT spectra to that of ref. 31 by using different functionals and basis sets (Gaussians *vs.* plane waves). Nevertheless, one needs to set a smaller linewidth of 0.02 eV to see the peak a closer to the experimental value. Peak a is really a doublet that has been assigned each to an electronic transition and to a vibronic replica.[10]

One can appreciate qualitative agreement between TDDFT and CNDOL results for transitions a, c, and e. CNDOL provides better peak positions for a, c, and e, and a less accurate description of the region over 5 eV. TDDFT provides transition energies matching the f and g band features, although incorrect intensities. CNDOL predicts transitions at a somewhat higher energy, 5.49 and 5.68 eV with oscillator strengths of 0.015 and 0.030 that are too weak to be appreciated in the plot. As commented above, the CNDO/S method overestimates the low-energy electron transitions in this case,[9,34] although it may be due to the relatively small active space employed at that time.

The different absorption functions have been rescaled to facilitate the comparison of the spectral shapes. As shown in Table 1, both TDDFT and CNDOL oscillator strengths are smaller than those of the experiments (see Table 2) in the case of the three strong bands. Their assigned[10] oscillator strengths are 0.37, 2.27, and 3.09 (roughly in proportion 1 : 6 : 8), respectively, in order of increasing energy. As we show in Table 2 and Fig. B1 in Appendix B, a proportion 1 : 9 : 20 results from a detailed fit of the spectrum, although the intensity of the first peak at 3.78 eV is uncertain because it is strongly influenced by two non-assigned transitions at close energies. The TDDFT approach gives oscillator strengths 0.417, 1.107, and 2.295 (in ratio 1 : 3 : 6), while CNDOL gives 0.429, 1.02, 2.10 (in ratio 2 : 5 : 10). Note that the TDDFT and CNDOL intensity ratio of the second to third peaks is close to our fit 9 : 20. The intensity of the c peak will be further discussed (Section 3.2). One problem is that TDDFT and CNDOL systematically give oscillator strengths lower than the experimental values in this system. However, the absorption intensities in *n*-hexane are likely to be enhanced by the interaction with the solvent. As discussed in ref. 63, the electromagnetic wave electric field is locally amplified due to a dielectric cavity effect and the reaction field to the molecular dipole. Hence, the measured absorption in a solvent must be corrected to obtain a representation of the absorption under vacuum. The corrected oscillator strengths are shown in

Table 2 Transition energies E, oscillator strengths f, and bandwidth parameters σ determined from the absorption spectrum of C_{60} in *n*-hexane.[10] The third column contains the results of a Lorentzian fit with solvent effects filtered with the Onsager correction.[63] $\hbar\gamma$ is the Lorentzian full width at half maximum. The units of E and σ are eV

Estimated[a] $E; f$	Gaussian fitting (this work) $E; f; \sigma$	Corrected fitting[b] $E; f; \sigma' = \frac{\hbar\gamma}{2\sqrt{2\ln 2}}$
3.04; 0.015	3.04; 0.002; 0.02	
3.30; ---	3.69; 0.46; 0.28	
3.78; **0.37**	**3.76; 0.24; 0.08**	3.78; 0.26; 0.09
4.06-	4.17; 0.096; 0.11	
4.35; 0.10	4.47; 0.49; 0.15	
4.84; **2.27**	**4.84; 2.27; 0.15**	4.87; 1.41; 0.13
5.46; 0.22	5.35; 0.25; 0.10	
5.88; **3.09**	**5.90; 4.90; 0.34**	6.04; 5.32; 0.36
6.36; ---	6.46; 0.44; 0.12	

[a] Ref. 10. [b] Ref. 63.

Table 2, showing reductions of the oscillator strengths as compared with the values in solution. An exception is the g band, where the corrected value is larger, and the transition energy is also modified by the solvent effect. However, the values for this band are affected by a significant oscillation in the real part of the polarizability, which affects the spectra accuracy deduced for this energy range. The c band was fitted in ref. 63 with only one Lorentzian. Hence, its oscillator strength of 0.26 can be compared with the value of 0.37 given by Leach *et al.*[10] However, let us notice when fitting with only one Lorentzian, one loses the broad band centered at 3.69 eV which adds a significant contribution to the total oscillator strength (see Fig. B1 in Appendix B). This issue will be discussed below.

3.2. $(C_{60})_N$ cluster results

Fig. 3 illustrates CNDOL results of singlet excited states of $(C_{60})_2$ dimer models. The cutoff energy criterion used to truncate the CIS matrix basis implies that 14644 SECs are needed to model the electron transitions of $(C_{60})_2$. Simulated absorption spectra were obtained under the same conditions as in Fig. 2, although in this case with a half width of 0.05 eV. Two different regions are shown in Fig. 3. The main plot displays the a peak region at the lower energy edge of the spectrum, while the inset shows the zone of the intense bands. The more significant effect observed in this dimer model is the appearance of a peak at 2.82 eV, which achieves intensity comparable to the peak a at 2.99 eV when the center–center distance is 10.02 Å. This result must be associated with the broken symmetry of the dimer system with respect to isolated C_{60} molecules. Both peaks in the dimer system appear arising from transitions to states delocalized across the whole dimer *i.e.* collective states. Fig. 3 also shows that peak a in dimer models tends to the same shape of that in the isolated C_{60}, where the distance (R) between fullerene centers increases to above 13 Å. This result is consistent with the localized

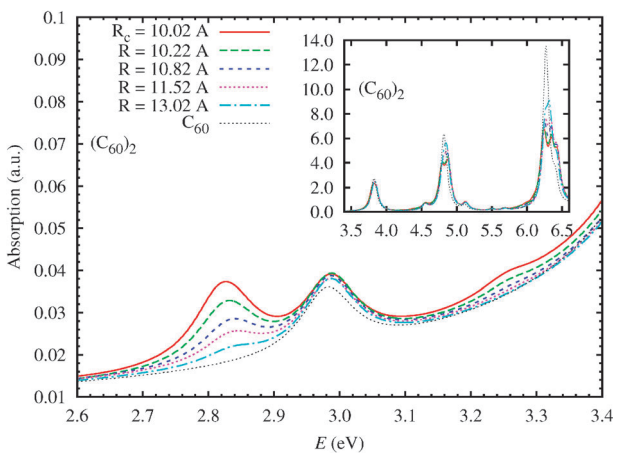

Fig. 3 CNDOL theoretical absorption spectra of $(C_{60})_2$ models compared with an isolated C_{60} model. The low energy region (2.6–3.4 eV) of the spectrum is in the main plot, while the zone of the intense bands is shown in the graphic inset. The line width used for band plotting is 0.05 eV. The distance (R) between fullerene centers in $(C_{60})_2$ models increases from the original in the fullerite crystal (R_c = 10.02 Å plotted in red) up to 13.02 Å.

character of electron transitions when fullerenes are at non-interacting distances. The above results are averaged over all the dimer orientations. For any given single dimer, the absorption is strongly polarized along the dimer axis, although the spectra with perpendicular polarization are still important.

The changes in the spectral bands above 3.5 eV (graphic inside in Fig. 3) are less significant with respect to the lowest energy region. The intense peaks e and g slightly change in the dimer models with respect to the isolated C_{60} absorption spectrum. In these cases, the optically active levels split and other states become weakly active. The oscillator strengths of peaks e and g are redistributed among two and three groups of states, respectively, separated by nearly 0.1 eV. With a simulated line width of 0.05 eV, peaks e and g look like a doublet and a triplet, while just a single peak and a peak with a shoulder are observed in the monomer absorption spectrum. However, as the observed bandwidth is much larger than 0.05 eV, these splittings cannot be noticed. The total calculated oscillator strength between 2 and 6.5 eV changes slightly from 8.07 for a pair of non-interacting monomers to 8.23 for the nearest dimer.

Larger cluster models of C_{60} hint more aspects of clustering influence on the absorption spectra. All electronic transitions of the whole studied region were obtained for every cluster model but $(C_{60})_{13}$. This largest model was used to study the effect of the cluster size over the spectral edge. CIS matrices involve 30 105, 48 000 and 86 400 SECs for $(C_{60})_N$ for N = 3, 4 and 6, respectively, while the low energy region of the $(C_{60})_{13}$ model spectrum was appropriately described using 27 208 SECs. Resulting calculated absorption spectra of all clusters are shown in Fig. 4. The lowest energy regions were simulated with a half bandwidth of 0.03 eV, whereas the other bands were simulated with a half bandwidth of 0.15 eV. The inset shows the relation between different selected half-width of the c, e and g bands with the number of molecules in the cluster. The widths of bands e and g tend to increase progressively when the cluster models become larger. As in the case of the dimer, the major spectral differences appear in the low energy region. In general, an increase in the cluster size implies more allowed electronic excitations in the low energy region of the spectrum.

It is noteworthy that the peak at around 2.85 eV for $(C_{60})_4$ and $(C_{60})_{13}$ resulted with a reduced intensity as compared with the cases of dimers and trimers. This must be another symmetry or shape effect, as the monomer, tetramer and tridecamer are *equant* objects, compared with the prolate dimer and the oblate trimer. Moreover, neither the $(C_{60})_4$ nor the $(C_{60})_{13}$ respective spectra appear polarized.

There are no experimental data on small fullerene clusters to compare with our simulation. Our results suggest the presence of small clusters in experiments, provided the fine structure of the absorption spectrum as measured in the range 2.5–3.2 eV. It has been suggested that the aggregates of C_{60} in water could be small spherical particles containing at least four C_{60} molecules.[25] The optical absorption spectra of them above 3.0 eV show broad bands that are slightly red-shifted (around 0.1 eV) in comparison with those of the *n*-hexane solution.[25,64] In addition, a low intensity and very broad band covers the spectral range between 2.3 and 3.0 eV. This spectral feature appears when the formation of C_{60} clusters is evident by

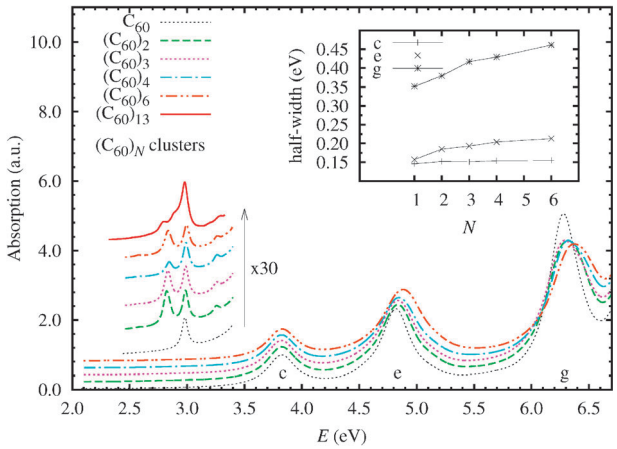

Fig. 4 CNDOL theoretical absorption spectra of $(C_{60})_N$ models. The low energy region of the spectrum has been inset amplified ×30 (left). The other inset (right) shows half-widths of the c, e and g bands for the $(C_{60})_N$ models where N = 2, 3, 4 and 6. All of $(C_{60})_N$ modeled absorption spectrum intensities have been divided by the number N of units. Absorption is shown in arbitrary units (a.u.) to allow comparisons.

electron microscopy studies,[25,64,65] as well as in the absorption spectra of the solid film.[18] This broad band reveals an activation of dipole-forbidden states by a number of possible causes, *e.g.*, clustering effects, solvent interaction, or dynamic geometry fluctuations. Nevertheless, our calculations suggest that optically active states in clusters could be localized in a narrow spectral range and cannot fully account for this broad band.

Fig. 5 shows the very interesting landscape of densities of singlet CIS states (DOS-CIS) for all of the studied clusters. DOS values are divided by the number of C_{60} units to normalize comparisons. These DOS-CIS are broad functions shown as a band representation in the whole range from 2.0 to 6.5 eV, illustrating the possibility of electron transitions assisted by some of the above mentioned mechanisms. Two clear behaviors are distinguished for the normalized DOS: (i) bands seem similar between 2 and about 3.5 eV; (ii) bands become increasingly higher with the size of clusters at higher energies. It can be easily understood as an excitonic process where every CIS excitation

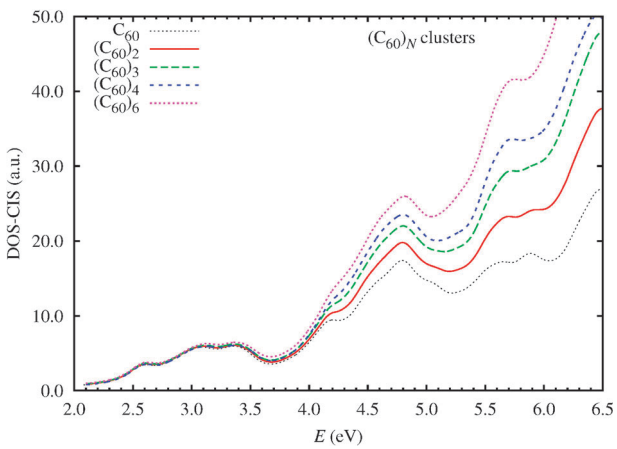

Fig. 5 CNDOL density of CIS states (DOS-CIS) obtained for the study systems. Each DOS is divided by the number of C_{60} units.

involves an electron and a hole, which can be located at any (or shared among several) of the C_{60} units. Thus, the total number of excited states is proportional to the square of the number of C_{60} units. Intermolecular excitations are present in DOS for energies higher than 3.5 eV.

The CNDO/S method has been previously used to study the nature of electronic excitations of a van der Waals dimer of C_{60}.[45] In that study, the CIS basis comprised 2000 SECs, and showed qualitatively the same results. The lowest states appear at around the same energies as the monomer transitions, although the oscillator strengths were not reported and the double peak structure at 2.8–3.0 eV was not revealed. On the other hand, the similarity of our absorption spectra of all the clusters above 3.5 eV reveals that intermolecular excitations are not dipole allowed. However, their presence must influence the spectrum by acting as additional relaxation channels for the allowed excitations. Hence, one expects an increment of the line broadening as a consequence of clustering effects. They may be already masked by the large bandwidth of the high-energy transitions, and it would be desirable to reveal these states by a direct method.

Let us consider the c band, which is fitted by two Gaussians centered at 3.69 and 3.76 eV (see Fig. B1 in Appendix B) and has oscillator strength amounts up to 0.70. If the Gaussian centered at 3.69 eV is not attributed to an electronic transition, the remaining contribution to the c band at 3.76 eV will be the only one transition with experimental oscillator strength smaller than the values from TDDFT and CNDOL calculations. Hence, we think that the broad band centered at 3.69 eV is also due to the 2^1T_{1u} level. A splitting of the 2^1T_{1u} level in 0.07 eV is incompatible with the symmetry of an isolated C_{60}. Our CNDOL calculations of the $(C_{60})_N$ clusters predict splits of this magnitude, *i.e.*, 0.05 eV. The fitted strengths have a ratio of 0.46/0.24 = 1.9, while the CNDOL calculations predict the ratios 1.0, 1.6, 1.8, and 1.4, for N = 2, 3, 4 and 6, respectively. Bandwidths of this doublet (σ = 0.28 and 0.08 eV) are remarkably different and we cannot offer a satisfactory explanation yet. For the sake of consistency, if clusters are present in *n*-hexane solution, a doublet fine structure should be observed at the low energy, as discussed above. It is possible that the solvent may affect differently the states of the doublet and they merge in a single peak, or that the oscillator strength may be transferred to one of the components. Additional simulations accounting for the solvent and clusters are necessary to clarify this issue, as well as experiments focused on this part of the spectrum. A plausible alternative is the Jahn–Teller effect, considering the triple degeneracy of the 2^1T_{1u} level, and the existence of multiple vibrational modes. Jahn–Teller effects are invoked to explain the absorption spectra in the range of 2–3 eV, where shifts of this magnitude are observed, as well as asymmetry in the bandwidths.[66] This effect may be present in a smaller measure for the bands e and g, and could be responsible for the shoulders d and f.

4. Conclusions

The CNDOL method predicts transition strengths for C_{60} in agreement with previous TDDFT calculations, although we attained better transition energy agreements with experimental results. Given that CNDOL is less demanding in computer

resources, we have advanced in the route of simulating collective phenomena observed in light absorption bands by clusters of C_{60}. In these cases, the results show that the density of states is enhanced by charge-transfer excitations in the region above 3.5 eV. However, the optical absorption due to dipole allowed transitions presents only minor changes due to clustering at the higher energies. Only the fine structure at the red edge of the spectrum appears modified by explicit collective effects, showing the possibility of new optically active states in clusters that could be significant for possible applications.

Appendix A: effect of the CIS basis size

Fig. A1 shows the effect of the size of the CIS basis, expressed in terms of the number of SECs. The 1200 SECs basis is roughly the size of the former CNDO/S calculations, and it is evident a bad description of the region above 6 eV. The Full CIS (with the atomic minimal basis set) provides a much better qualitative and quantitative agreement with the experiments. The 4621 SECs basis includes all the SECs with energy smaller than 13.2 eV, plus a few SECs added to complete the excited state shells present in the basis. This basis is qualitatively similar to the Full CIS basis, for a much lower computational cost, which is needed for the study of C_{60} clusters.

Appendix B: fit of the spectrum

Fig. B1 shows the experimental data and fits of light absorption by C_{60} in *n*-hexane solution. The thick lines show the fitted spectrum and the thin lines show the contribution of each transition. The dotted lines are the curve with the parameters estimated by Leach *et al.*[10] The oscillator strength fitted for the allowed transitions at 3.76, 4.84 and 5.90 eV are 0.24, 2.27 and 4.90 (proportion 1 : 9 : 20), respectively. Note the broad band b centered at 3.69 eV. Its presence decreases the strength of the transition at 3.76 eV. If it is adjusted with a simple Gaussian, the height of peak c is well reproduced, but there is a considerable amount of oscillator strength unaccounted, which is associated to the feature b. Also note that the peak e, at 4.84 eV, can be described by a single Gaussian and is little affected by the transition d. Hence, peak e can be used to gauge the fitting procedure, and we have fixed its oscillator strength at 2.27 to agree with ref. 10.

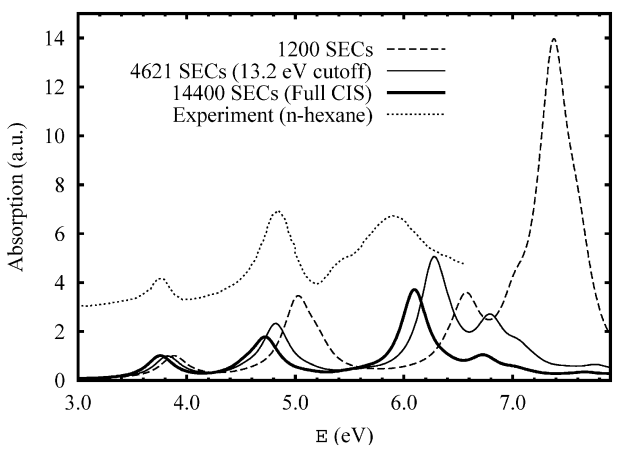

Fig. A1 Effect of the size of the CIS basis over the CNDOL calculated spectrum of C_{60}.

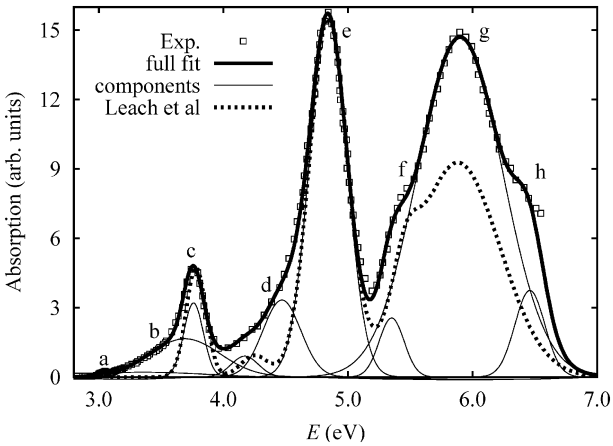

Fig. B1 Experimental data and fits of the absorption spectrum by C_{60} in *n*-hexane solution. In the fit we have fixed the 2.27 oscillator strength. Thin solid lines show the Gaussian components of the fitted function.

Acknowledgements

This work was supported by the MICIN of Spain (CTQ2010-19232), the Spanish Agency for International Cooperation for Development (AECID) (D/030752/10 and A1/035856/11) and the Ministry of Education of Spain (SB2010-0119). E.M.-P. thanks R. Gebauer for many useful comments on TDDFT and optical properties. A.D. acknowledges the financial support from the FP7 Marie Curie IIF project HY-SUNLIGHT: 252906.

References

1 T. M. Clarke and J. R. Durrant, *Chem. Rev.*, 2010, **110**, 6736–6767.
2 M. Ohtani and S. Fukuzumi, *Fullerenes, Nanotubes, Carbon Nanostruct.*, 2010, **18**, 251–260.
3 P. Chawla, V. Chawla, R. Maheshwari, S. A. Saraf and S. K. Saraf, *Mini-Rev. Med. Chem.*, 2010, **10**, 662–677.
4 D. V. Schur, S. Y. Zaginaichenko, A. F. Savenko, V. A. Bogolepov, N. S. Anikina, A. D. Zolotarenko, Z. A. Matysina, T. N. Veziroglu and N. E. Skryabina, *Int. J. Hydrogen Energy*, 2011, **36**, 1143–1151.
5 K. R. S. Chandrakumar and S. K. Ghosh, *Nano Lett.*, 2007, **8**, 13–19.
6 X. Liu, J. e. Yang, C. Zhou, X. Yin, H. Liu, Y. Li and Y. Li, *Phys. Chem. Chem. Phys.*, 2011, **13**, 1984–1989.
7 B. Lampe and T. Koslowski, *Phys. Chem. Chem. Phys.*, 2011, **13**, 16247–16253.
8 Y. He and Y. Li, *Phys. Chem. Chem. Phys.*, 2011, **13**, 1970–1983.
9 G. Orlandi and F. Negri, *Photochem. Photobiol. Sci.*, 2002, **1**, 289–308.
10 S. Leach, M. Vervloet, A. Desprès, E. Breheret, J. P. Hare, T. J. Dennis, H. W. Kroto, R. Taylor and D. R. M. Walton, *Chem. Phys.*, 1992, **160**, 451–466.
11 R. E. Haufler, Y. Chai, L. P. F. Chibante, M. R. Fraelich, R. B. Weisman, R. F. Curl and R. E. Smalley, *J. Chem. Phys.*, 1991, **95**, 2197.
12 Q. Gong, Y. Sun, Z. Huang, X. Zhou, Z. Gu and D. Qiang, *J. Phys. B: At., Mol. Opt. Phys.*, 1996, **29**, 4981.
13 A. Sassara, G. Zerza, M. Chergui and S. Leach, *Astrophys. J., Suppl. Ser.*, 2001, **135**, 263–273.
14 J. Catalán and P. Pérez, *Fullerenes, Nanotubes, Carbon Nanostruct.*, 2002, **10**, 171.
15 J. D. Close, F. Federmann, K. Hoffmann and N. Quaas, *Chem. Phys. Lett.*, 1997, **276**, 393–398.

16 N. Sogoshi, Y. Kato, T. Wakabayashi, T. Momose, S. Tam, M. E. DeRose and M. E. Fajardo, *J. Phys. Chem. A*, 2000, **104**, 3733–3742.
17 W. Kratschmer, L. D. Lamb, K. Fostiropoulos and D. R. Huffman, *Nature*, 1990, **347**, 354–358.
18 Y. Wang, J. M. Holden, A. M. Rao, P. C. Eklund, U. D. Venkateswaran, D. Eastwood, R. L. Lidberg, G. Dresselhaus and M. S. Dresselhaus, *Phys. Rev. B: Condens. Matter Mater. Phys.*, 1995, **51**, 4547–4556.
19 A. Sassara, G. Zerza, M. Chergui, F. Negri and G. Orlandi, *J. Chem. Phys.*, 1997, **107**, 8731.
20 A. Sassara, G. Zerza and M. Chergui, *J. Phys. B: At., Mol. Opt. Phys.*, 1996, **29**, 4997.
21 A. Sassara, G. Zerza and M. Chergui, *Chem. Phys. Lett.*, 1996, **261**, 213–220.
22 D. J. van den Heuvel, I. Y. Chan, E. J. J. Groenen, J. Schmidt and G. Meijer, *Chem. Phys. Lett.*, 1994, **231**, 111–118.
23 D. J. van den Heuvel, I. Y. Chan, E. J. J. Groenen, M. Matsushita, J. Schmidt and G. Meijer, *Chem. Phys. Lett.*, 1995, **233**, 284–290.
24 A. L. Smith, *J. Phys. B: At., Mol. Opt. Phys.*, 1996, **29**, 4975.
25 L. Bulavin, I. Adamenko, Y. Prylutskyy, S. Durov, A. Graja, A. Bogucki and P. Scharff, *Phys. Chem. Chem. Phys.*, 2000, **2**, 1627–1629.
26 J. D. Fortner, D. Y. Lyon, C. M. Sayes, A. M. Boyd, J. C. Falkner, E. M. Hotze, L. B. Alemany, Y. J. Tao, W. Guo, K. D. Ausman, V. L. Colvin and J. B. Hughes, *Environ. Sci. Technol.*, 2005, **39**, 4307–4316.
27 X. Chang and P. J. Vikesland, *Environ. Sci. Technol.*, 2011, **45**, 9967–9974.
28 E. Westin, A. Rosen, G. T. Velde and E. J. Baerend, *J. Phys. B: At., Mol. Opt. Phys.*, 1996, **29**, 5087–5113.
29 S. Iglesias-Groth, A. Ruiz, J. Breton and J. M. Gomez Llorente, *J. Chem. Phys.*, 2002, **116**, 10648–10655.
30 Miguel A. L. Marques, Carsten A. Ullrich, Fernando Nogueira, Angel Rubio, Kieron Burke and E. K. U. Gross, *Time-Dependent Density Functional Theory*, Springer, Berlin/Heidelberg, 2006.
31 R. Bauernschmitt, R. Ahlrichs, F. H. Hennrich and M. M. Kappes, *J. Am. Chem. Soc.*, 1998, **120**, 5052–5059.
32 A. Tsolakidis, D. Sánchez-Portal and R. M. Martin, *Phys. Rev. B: Condens. Matter Mater. Phys.*, 2002, **66**, 235416.
33 J. Del Bene and H. H. Jaffe, *J. Chem. Phys.*, 1968, **48**, 1807–1813.
34 F. Negri, G. Orlandi and F. Zerbetto, *J. Chem. Phys.*, 1992, **97**, 6496.
35 T. Hara, S. Narita and T.-i. Shibuya, *Fullerene Sci. Technol.*, 1995, **3**, 459–467.
36 D. Rocca, R. Gebauer, Y. Saad and S. Baroni, *J. Chem. Phys.*, 2008, **128**, 154105.
37 P. Koval, D. Foerster and O. Coulaud, *J. Chem. Theory Comput.*, 2010, **6**, 2654–2668.
38 L. Rincon, A. Hasmy, C. A. Gonzalez and R. Almeida, *J. Chem. Phys.*, 2008, **129**, 044107.
39 B. M. Wong and T. H. Hsieh, *J. Chem. Theory Comput.*, 2010, **6**, 3704–3712.
40 T. Minami, M. Nakano and F. Castet, *J. Phys. Chem. Lett.*, 2011, **2**, 1725–1730.
41 A. V. Nikolaev, I. V. Bodrenko and E. V. Tkalya, *Phys. Rev. A: At., Mol., Opt. Phys.*, 2008, **77**, 012503.
42 D. M. Guldi, G. M. A. Rahman, V. Sgobba and C. Ehli, *Chem. Soc. Rev.*, 2006, **35**, 471–487.
43 A. A. Voityuk and M. Duran, *J. Phys. Chem. C*, 2008, **112**, 1672–1678.
44 R. Zalesny, O. Loboda, K. Iliopoulos, G. Chatzikyriakos, S. Couris, G. Rotas, N. Tagmatarchis, A. Avramopoulos and M. G. Papadopoulos, *Phys. Chem. Chem. Phys.*, 2010, **12**, 373–381.
45 P. R. Surjan, L. Udvardi and K. Nemeth, *Synth. Met.*, 1996, **77**, 107–110.
46 L. A. Montero, L. Alfonso, J. R. Alvarez and E. Perez, *Int. J. Quantum Chem.*, 1990, **37**, 465–483.
47 L. A. Montero-Cabrera, U. Röhrig, J. A. Padron-García, R. Crespo-Otero, A. L. Montero-Alejo, J. M. García de la Vega, M. Chergui and U. Röthlisberger, *J. Chem. Phys.*, 2007, **127**, 145102.
48 M. E. Fuentes, B. Peña, C. Contreras, A. L. Montero, R. Chianelli, M. Alvarado, R. Olivas, L. M. Rodríguez, H. Camacho and L. A. Montero-Cabrera, *Int. J. Quantum Chem.*, 2008, **108**, 1664–1673.
49 A. L. Montero-Alejo, M. E. Fuentes, E. Menéndez-Proupin, W. Orellana, C. F. Bunge, L. A. Montero and J. M. García de la Vega, *Phys. Rev. B: Condens. Matter Mater. Phys.*, 2010, **81**, 235409.
50 J. A. Pople and G. A. Segal, *J. Chem. Phys.*, 1966, **44**, 3289–3296.
51 N. Mataga and K. Nishimoto, *Z. Phys. Chem. (Leipzig)*, 1957, **13**, 140–157.
52 K. Nishimoto and N. Mataga, *Z. Phys. Chem. (Leipzig)*, 1957, **12**, 335–338.
53 R. Pariser, *J. Chem. Phys.*, 1953, **21**, 568–569.
54 A. Szabo and N. S. Ostlung, *Modern quantum chemistry: introduction to advanced electronic structure theory*, Dover Publications Inc., New York, 1996.
55 D. L. Dorset and M. P. McCourt, *Acta Crystallogr., Sect. A: Found. Crystallogr.*, 1994, **50**, 344–351.
56 P. Giannozzi, S. Baroni, N. Bonini, M. Calandra, R. Car, C. Cavazzoni, D. Ceresoli, G. L. Chiarotti, M. Cococcioni, I. Dabo, A. Dal Corso, S. de Gironcoli, S. Fabris, G. Fratesi, R. Gebauer, U. Gerstmann, C. Gougoussis, A. Kokalj, M. Lazzeri, L. Martin-Samos, N. Marzari, F. Mauri, R. Mazzarello, S. Paolini, A. Pasquarello, L. Paulatto, C. Sbraccia, S. Scandolo, G. Sclauzero, A. P. Seitsonen, A. Smogunov, P. Umari and R. Wentzcovitch, *J. Phys.: Condens. Matter*, 2009, **21**, 395502.
57 J. P. Perdew, K. Burke and M. Ernzerhof, *Phys. Rev. Lett.*, 1996, **77**, 3865.
58 N. Marzari, D. Vanderbilt, A. De Vita and M. C. Payne, *Phys. Rev. Lett.*, 1999, **82**, 3296.
59 K. Hedberg, L. Hedberg, D. S. Bethune, C. A. Brown, H. C. Dorn, R. D. Johnson and M. De Vries, *Science*, 1991, **254**, 410–412.
60 A. K. Soper, W. I. F. David, D. S. Sivia, T. J. S. Dennis, J. P. Hare and K. Prassides, *J. Phys.: Condens. Matter*, 1992, **4**, 6087–6094.
61 W. Branz, N. Malinowski, A. Enders and T. P. Martin, *Phys. Rev. B: Condens. Matter Mater. Phys.*, 2002, **66**, 094107.
62 M. Braga, S. Larsson, A. Rosen and A. Volosov, *Astron. Astrophys.*, 1991, **245**, 232–238.
63 J. U. Andersen and E. Bonderup, *Eur. Phys. J. D*, 2000, **11**, 435–448.
64 P. Scharff, K. Risch, L. Carta-Abelmann, I. M. Dmytruk, M. M. Bilyi, O. A. Golub, A. V. Khavryuchenko, E. V. Buzaneva, V. L. Aksenov, M. V. Avdeev, Y. I. Prylutskyy and S. S. Durov, *Carbon*, 2004, **42**, 1203–1206.
65 G. V. Andrievsky, V. K. Klochkov, E. L. Karyakina and N. O. McHedlov-Petrossyan, *Chem. Phys. Lett.*, 1999, **300**, 392–396.
66 I. D. Hands, J. L. Dunn, C. A. Bates, M. J. Hope, S. R. Meech and D. L. Andrews, *Phys. Rev. B: Condens. Matter Mater. Phys.*, 2008, **77**, 115445.

